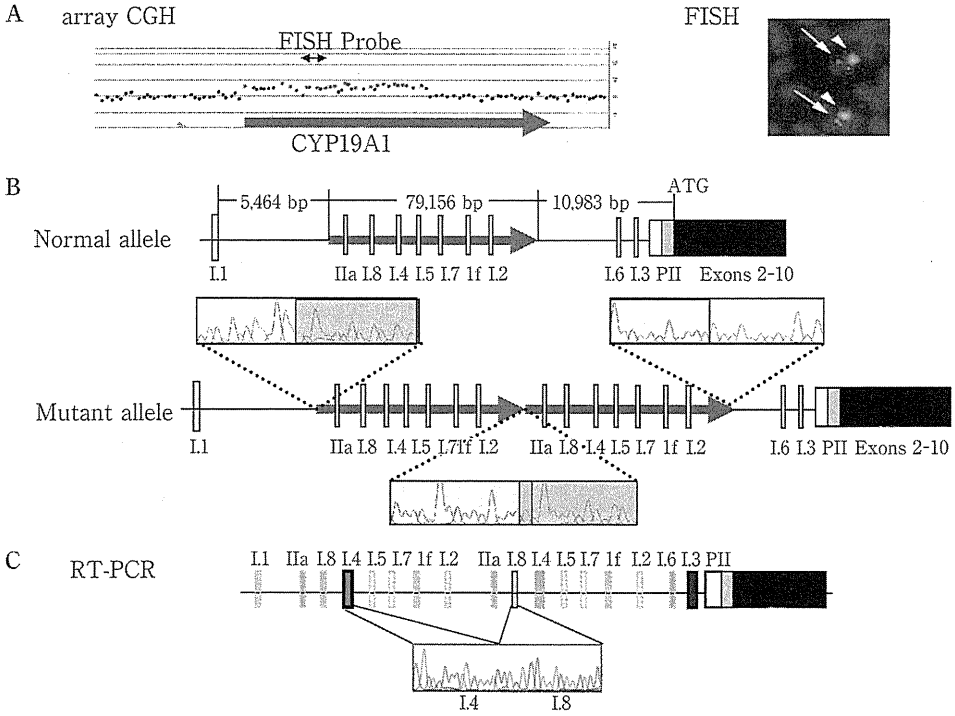

図 4　アロマターゼ過剰症家系 A と B における遺伝子異常

A：アレイ CGH 解析(左)と FISH 解析(右)。*CYP19A1* のプロモーター領域のヘテロ接合性重複が同定された。**B**：ゲノム構造異常。*CYP19A1* エクソン 1 のうち七つを包含するタンデム重複。Fusion point は反復配列外にあり，1 塩基の相同性を有する。**C**：mRNA 解析。5'側にエクソン I.4，3'側にエクソン I.8 が結合した mRNA クローンが同定された。このクローンの存在は遠位に増えたエクソン I.4 からも転写が生じていることを示唆する。

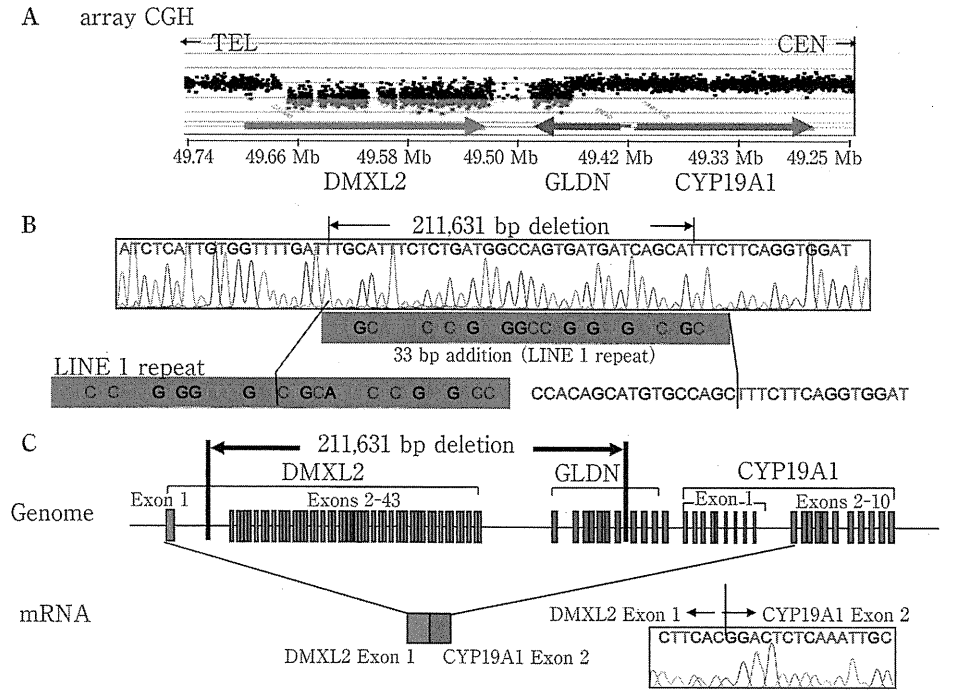

図 5　アロマターゼ過剰症家系 C における遺伝子異常

A：アレイ CGH 解析。*CYP19A1* 上流領域のヘテロ接合性欠失が同定された。**B**：ゲノム構造異常。*DMXL2* エクソン 2-43 と *GLDN* エクソン 5-10 を包含する欠失が同定された。切断点は一方は LINE 1 配列内，他方は反復配列外にあり，33 塩基の由来不明の塩基配列の挿入を伴う。**C**：mRNA 解析。*DMXL2-CYP19A1* キメラ mRNA クローンが同定された。

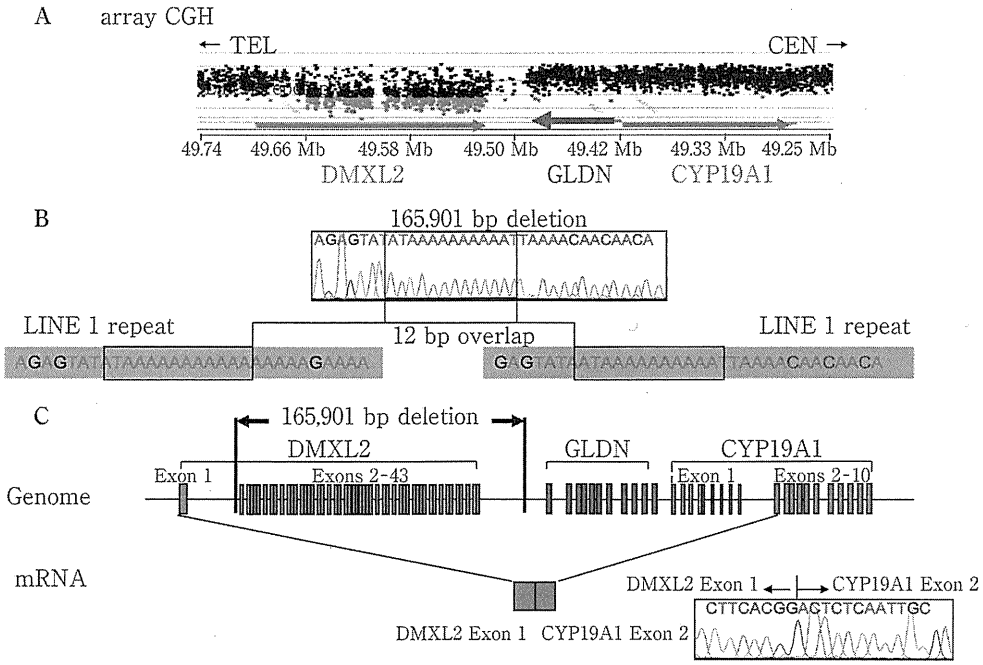

図 6 アロマターゼ過剰症家系 D-F における遺伝子異常

A：アレイ CGH 解析。*CYP19A1* 上流領域のヘテロ接合性欠失が同定された。**B**：ゲノム構造異常。*DMXL2* エクソン 2-43 を包含する欠失が同定された。切断点はともに LINE 1 配列内にあり，12 塩基の重複を伴う。**C**：mRNA 解析。*DMXL2-CYP19A1* キメラ mRNA が同定された。

このクローンの存在は，欠失によって *DMXL2* エクソン 1 と *CYP19A1* エクソン 2 の間でスプライスが生じ，その結果，*CYP19A1* 翻訳領域が *DMXL2* プロモーターによる制御を受けるようになったことを示唆する。

家系 D-F では *CYP19A1* スタートコドンから 174,315 bp 離れた領域に 165,901 bp の欠失が同定された(図 6A，B)。この欠失は *DMXL2* エクソン 2-43 を包含していた。この欠失の二つの切断点はともに LINE 1 配列内にあり，12 塩基の重複を伴っていた。これらの家系では家系 C と同様の機序で *DMXL2-CYP19A1* キメラ遺伝子が形成され，アロマターゼ遺伝子過剰発現が生じたと推測される(図 6C)。

患者の遺伝子型-表現型解析から，遺伝子変異パターンと臨床症状の重症度の間にはある程度の相関があることが明らかとなった。すなわち，重複陽性患者では比較的軽度の，欠失陽性患者では中等度の症状が認められた。また，過去に報告された逆位陽性患者では重度の乳房腫大や骨年齢促進が生じることが見出されている。このことは，本症の重症度が *CYP19A1* に結合したプロモーターの機能と構造を反映することを示唆する。生理的 *CYP19A1* プロモーターの重複は通常の *CYP19A1* 発現部位に限局した過剰発現を招くため，比較的少量のアロマターゼ蛋白過剰産生を招くと推測される。一方，欠失例と逆位例のキメラ遺伝子では，広範囲発現遺伝子のプロモーターによる多臓器・組織での *CYP19A1* 遺伝子発現増加が生じ，比較的多量のアロマターゼ蛋白が産生されると予想される。さらに，*CYP19A1* エクソン 2 と *DMXL2* エクソン 1 の両者に翻訳開始コドンを有する *DMXL2-CYP19A1* キメラ遺伝子は，アロマターゼ蛋白のほかに *DMXL2* 翻訳開始コドンから読み取られる無機能蛋白をコードするが，エクソン 1 に翻訳開始コドンを持たない逆位例のキメラ遺伝子ではアロマターゼ蛋白のみが産生される。このため，アロマターゼ蛋白産生量は *DMXL2-CYP19A1* キメラ遺伝子より逆位例のキメラ遺伝子においてはるかに多いと考えられる。このようなプロモーター構造の違い(融合プロモーターを有するエクソン上の翻訳開始点の有無)が，欠失陽性患者と逆位陽性患者の重症度の差に寄与している可能性がある。さらに，増加したエストロゲンによる負のフィードバックは生理的 *CYP19A1* プロモーターの重複では認められ

るが，欠失や逆位による非生理的プロモーターでは存在しない，あるいは乏しいと推測され，これも臨床像の違いに寄与していると思われる。

以上の成績は，生理的プロモーターの重複および遺伝子上流の微小欠失が遺伝子過剰発現を招き，ヒトの遺伝病の原因となることを世界で初めて示すものである。なお，切断点の塩基配列解析から，家系AとBの重複はfork stalling and template switching(FoSTeS)によって説明可能であり，家系Cと家系D-Fの欠失はそれぞれnon-homologous end joiningとnon-allelic recombinationに一致することが見出された。このことは，本症の発症にDNA複製エラーと組換え異常に起因する多様な染色体微細構造異常が関与することを示唆する。このような多様な構造異常が*CYP19A1*周辺領域に認められることから，この染色体領域にはゲノム微細構造異常を生じやすいなんらかの特異的モチーフが存在すると推測される。

結　語

近年，小児内分泌疾患の発症にさまざまなコピー数異常が関与することが明確となった。このようなゲノム微細構造異常は小児内分泌疾患以外の疾患の発症にも関与する可能性がある。

●文　献

1) 緒方勤：ターナー症候群の遺伝学，メディカルレビュー社，東京，2003
2) Fukami M, Dateki S, Kato F et al：*J Hum Genet* **53**(5)：454-459, 2008
3) Shozu M, Sebastian S, Takayama K et al：*N Engl J Med* **348**：1855-1865, 2003
4) Demura M, Martin RM, Shozu M et al：*Hum Mol Genet* **16**：2529-2541, 2007
5) Fukami M, Shozu M, Soneda S et al：*J Clin Endocrinol Metab* **96**(6)：E1035-1043, 2011

遺伝性女性化乳房症6家系における疾患成立機序と臨床像の解明

国立成育医療研究センター[1] 鳥取大学[2] 山梨大学[3] 大阪警察病院[4]
名古屋第二赤十字病院[5] Tubingen大学[6] 千葉大学[7]

深見 真紀[1] 曽根田 瞬[1] 加藤芙弥子[1] 花木 啓一[2] 神埼 晋[2]
大山 建司[3] 佐野 友昭[3] 西垣 敏紀[4] 稲垣 朱実[5] 高木 博史[5]
Gerhard Binder[6] 横谷 進[1] 堀川 玲子[1] 生水真紀夫[7] 緒方 勤[1]

背 景

アロマターゼは、エストロゲンをアンドロゲンへと変換する酵素である。アロマターゼ遺伝子(*CYP19A1*)は、15番染色体上に存在し、すくなくとも11個の非翻訳エクソン1と翻訳領域であるエクソン2-10から成る。各々のエクソン1は、組織特異的プロモーターとして機能している。通常、*CYP19A1*の発現は、胎盤や卵巣など一部の組織を除いて低いレベルに制御されている。

*CYP19A1*の過剰発現は、遺伝性女性化乳房(HG)を招く。HGは、男性患者における乳房腫大、骨年齢促進と最終身長低下、性腺機能低下を主徴とする常染色体性優性遺伝疾患である。女性患者の多くは無症状であるが、一部の症例では月経異常や思春期早発などが認められる。

2003年、Shozuらにより、HG患者において15番染色体逆位が同定された[1]。その後、これまでに2家系と2孤発例の患者において逆位が同定されている[2]。mRNAの解析から、これら逆位陽性患者では、*CYP19A1*と近隣に位置する広範囲発現遺伝子のキメラ形成が*CYP19A1*過剰発現の原因であることが明らかとなっている[1),2)]。しかし、HG患者の詳細な臨床像、および、逆位陰性HG患者における発症機序は解明されていない。今回われわれは、HG患者6家系の分子遺伝学的／臨床的解析を行い、これらの点を解明した。

1．対 象

臨床的にHGと診断された男性6家系18例(家系A-F)。家系Eはドイツ人、他の家系は日本人である。乳房腫大の程度は、家系AとBにおいてやや軽度であった。一部の症例では、精巣容積低下など軽度の二次性徴進行不全を認めた。成人患者の妊孕性(精子形成)は保持されていた。血中ホルモン検査では、estrone(E_1)高値、estradiol(E_2)／testosterone(T)比高値、FSH優位のゴナドトロピン分泌不全が認められた。皮膚線維芽細胞の解析では、*CYP19A1* mRNA量増加とアロマターゼ酵素活性亢進が確認された。

2．方 法

1. *CYP19A1*翻訳領域の塩基配列解析

本研究の遺伝子解析は、国立成育医療研究センター倫理員会において承認されている。インフォームドコンセントを得たのち、ゲノムDNAを採取し、*CYP19A1*翻訳領域であるエクソン2-10をPCRで増幅した。直接塩基配列決定を行い、アミノ酸変化を伴う変異の有無について検討した。

2. ゲノム構造異常解析

Comparative genomic hybridization(CGH)法により、*CYP19A1*近傍のゲノム構造異常の有無について検討した。本研究では、15q11.2-q26.3領域に対応する90,000のプローブと他の染色体領域に対応する約10,000のリファレンスプローブを搭載したカスタムマイクロアレイを作成し、解析に使用した(Agilent Technologies, Palo Alto, CA)。欠失や重複が同定された場合は、確認のためlong-PCRでプローブを作成し、FISHを行った。また、切断点周辺に設計したプライマーを用いたlong PCR産物の直接塩基配列決定により、切断点の位置と構造を決定した。

3. mRNA解析

患者末梢血または皮膚線維芽細胞からmRNAを抽出し、5'-rapid amplification of cDNA ends(5'-RACE)法により、*CYP19A1*翻訳領域に結合しているプロモーターを同定した。

3．結 果

1. *CYP19A1*翻訳領域の塩基配列解析

全患者において、*CYP19A1*翻訳領域には変異が同定されなかった。

2. ゲノム構造異常解析

家系A-Fにおいて、*CYP19A1*遺伝子翻訳領域上流にヘテロ接合性ゲノム構造異常が同定された。これらの異常は、CGHによって見出され、FISHで確認された。さらに、Long PCR産物の塩基配列決定により、切断点が決定された。

家系AとBでは*CYP19A1*スタートコドンから10,983bp離れた領域に79,156bpの大きさのタンデム重複が同定された(図1A, B)。この領域は、*CYP19A1*の

11 の非翻訳エクソン 1 のうちの 7 つ(エクソン IIa, 1.8, 1.4, 1.5, 1.7, 1f, 1.2)を包含していた。この重複の切断点は、反復配列外にあり、1 塩基の相同性を有していた。

家系 C では、*CYP19A1* スタートコドンから 141,758 bp 離れた領域に 211,631 bp の欠失が同定された(図 2A, B)。この欠失は、隣接遺伝子 *DMXL2* エクソン 2-43 と *GLDN* エクソン 5-10 を包含していた。この欠失の切断点は、一方は LINE 1 配列内、他方は反復配列外にあり、33 塩基の塩基配列の挿入を伴っていた。

家系 D-F では *CYP19A1* スタートコドンから 174,315 bp 離れた領域に 165,901 bp の欠失が同定された(図 3A, B)。この欠失は、*DMXL2* エクソン 2-43 を包含していた。この欠失の 2 つの切断点はともに LINE 1 配列内にあり、12 塩基の重複を伴っていた。

3. mRNA 解析

5'-RACE により、患者の *CYP19A1* mRNA について検討した。家系 A と B では、*CYP19A1* エクソン 1 のうちの 1 つを有する正常な mRNA クローンのみが検出された。一方、5'-RACE 産物をテンプレートとして、各エクソン 1 に位置するプライマーを用いて行った PCR では、5' 側にエクソン 1.4、3' 側にエクソン 1.8 が結合したクローンが得られた(図 1C)。このクローンはスプライスエラーによって生じた産物であると推測される。このクローンの存在は、重複によって遠位に増えた 1.4 プロモーターから転写が生じていることを示すものである。

家系 C-F では、*CYP19A1* エクソン 1 のうちの 1 つを有するクローンのほか、*DMXL2* エクソン 1 を含む *DMXL2-CYP19A1* キメラクローンが得られた(図 2C, 3C)。このキメラ mRNA は、全 5'-RACE 産物の 2-5% を占めていた。このクローンの存在は、欠失によって *DMXL2* エクソン 1 と *CYP19A1* エクソン 2 の間でスプライスが生じ、その結果 *CYP19A1* 翻訳領域が *DMXL2* プロモーターによる制御を受けるようになったことを示唆する。

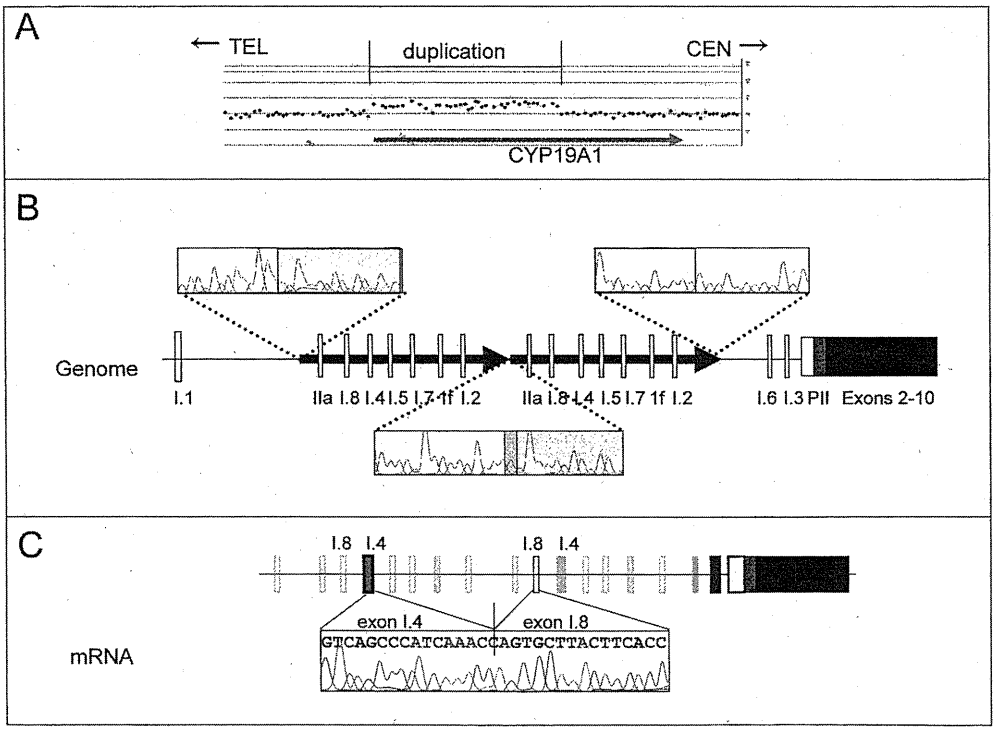

図 1. 家系 A と B における遺伝子異常
A：CGH アレイ解析。*CYP19A1* の一部のヘテロ接合性重複。
B：ゲノム構造異常。*CYP19A1* エクソン 1 のうち 7 つを包含するタンデム重複。切断点は、反復配列外にあり、1 塩基の相同性を有する。
C：mRNA 解析。5' 側にエクソン 1.4、3' 側にエクソン 1.8 が結合した mRNA クローン。

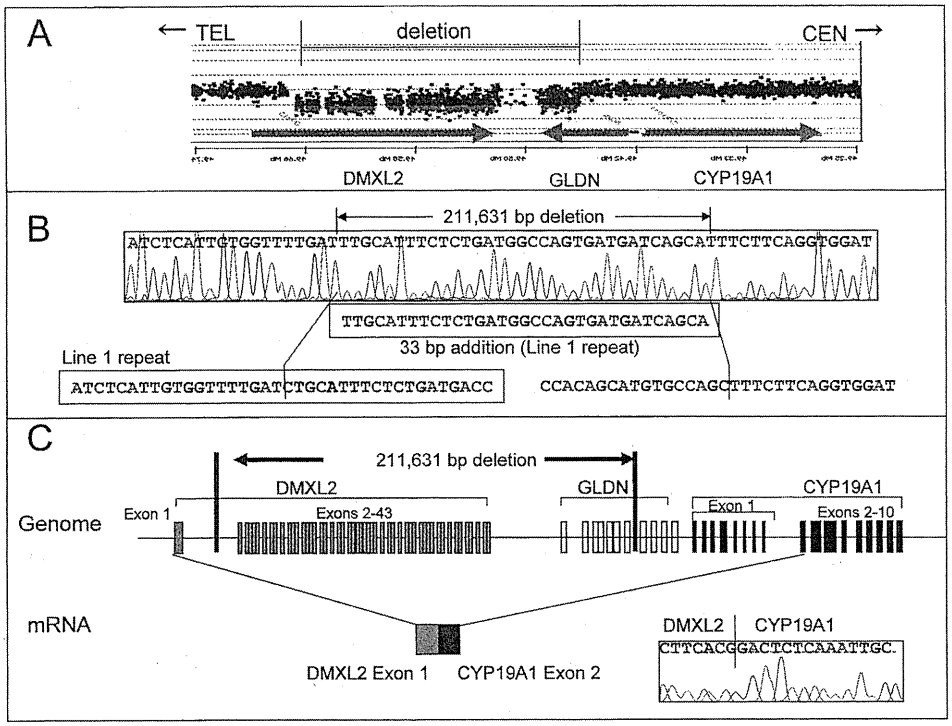

図 2. 家系 C における遺伝子異常
A：CGH アレイ解析。*CYP19A1* 上流領域のヘテロ接合性欠失。
B：ゲノム構造異常。*DMXL2* エクソン 2-43 と *GLDN* エクソン 5-10 を包含する欠失。切断点は、一方は LINE 1 配列内、他方は反復配列外にあり、33 塩基の塩基配列の挿入を伴う。
C：mRNA 解析。5'-RACE で同定された *DMXL2-CYP19A1* キメラ mRNA。

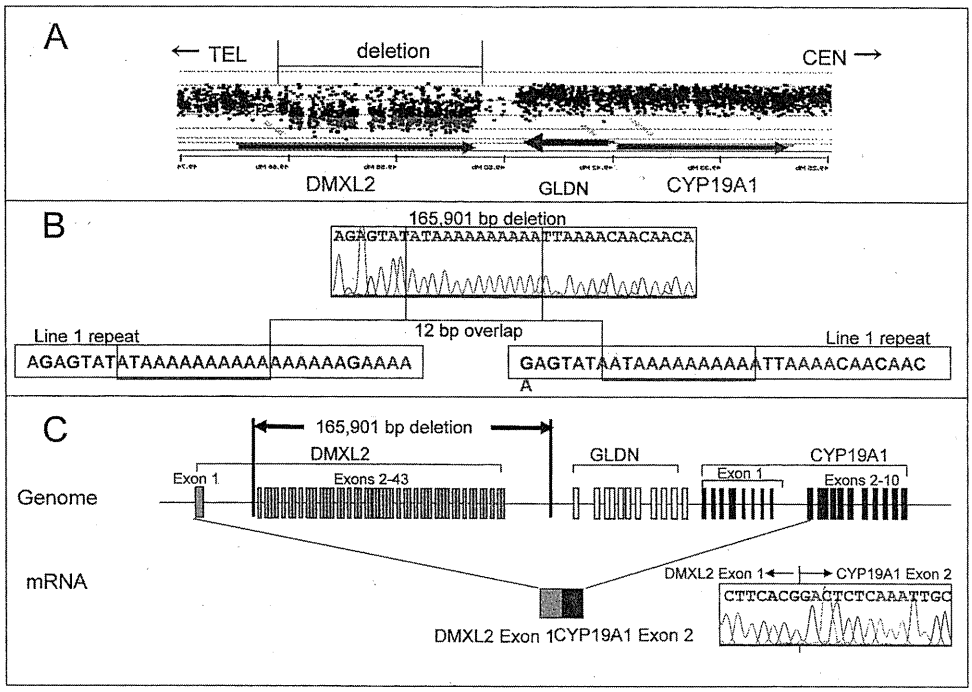

図 3. 家系 D-F における遺伝子異常
A：CGH アレイ解析。*CYP19A1* 上流領域のヘテロ接合性欠失。
B：ゲノム構造異常。*DMXL2* エクソン 2-43 を包含する欠失。切断点はともに LINE 1 配列内にあり、12 塩基の重複を伴う。
C：mRNA 解析。5'-RACE で同定された *DMXL2-CYP19A1* キメラ mRNA。

4．考　察

われわれは、HG 6家系の解析を行い、2家系で *CYP19A1* プロモーター領域の重複、4家系で *CYP19A1* 上流の微小欠失を同定した。重複陽性患者では、*CYP19A1* プロモーター数増加に起因する転写効率増加によって、アロマターゼ過剰産生が生じたと推測される。一方、欠失陽性患者では、*DMXL2* プロモーターの獲得による *CYP19A1* の異所性発現とプロモーター数増加による転写効率増加がアロマターゼ過剰産生の原因であると推測される。この成績は、生理的プロモーターの重複および遺伝子上流の微小欠失が、遺伝子過剰発現を招き、ヒトの遺伝病の原因となることを世界で初めて示すものである。このようなゲノム構造異常は、他の遺伝疾患の発症にも関与している可能性がある。

本研究の成績は、HGの発症にDNA複製エラーと組み換え異常に起因する多様な染色体微細構造異常が関与することを示唆する。すなわち、家系AとBの重複はfork stalling and template switching（FoSTes）によって説明可能であり、家系Cと家系D-Fの欠失はそれぞれnon-homologous end joiningとnon-allelic homologous recombinationに一致する。このような多様な構造異常が *CYP19A1* 周辺領域に認められることから、この染色体領域にはゲノム微細構造異常を生じやすい特異的モチーフが存在すると推測される。

なお、患者の乳房腫大と骨年齢促進の程度には症例間差異が存在し、重複陽性患者と欠失陽性患者の臨床症状は、既報の染色体逆位陽性患に比較して軽度であった。とくに家系AとBにおいて軽度の臨床症状が認められた。このことは、本症の重症度が *CYP19A1* に結合したプロモーターの機能と構造を反映することを示唆する。すなわち、生理的 *CYP19A1* プロモーターの重複は、通常の *CYP19A1* 発現部位に限局した過剰発現を招くため、比較的少量のアロマターゼ蛋白過剰産生を招くと推測される。一方、欠失例と逆位例のキメラ遺伝子形成には広範囲発現遺伝子のプロモーターが関与するため、多量のアロマターゼ蛋白が産生されると予想される。さらに、*DMXL2* エクソン1には翻訳開始コドンが存在するため、*DMXL2-CYP19A1* キメラ遺伝子はアロマターゼ蛋白のほかに *DMXL2* 翻訳開始コドンから読みとられる無機能蛋白をコードするが、エクソン1に翻訳開始コドンを持たない逆位例のキメラ遺伝子ではアロマターゼ蛋白のみが産生される。このようなプロモーター構造の違いが、欠失陽性患者と逆位陽性患者の重症度の差に寄与している可能性がある。事実、5'-RACE産物のなかでキメラmRNAの占める割合は、欠失例では数%であるのに対し、既報の逆位例では80-90%であった[2]。

結　語

本研究によって、プロモーター領域の重複と遺伝子上流の微小欠失が遺伝子過剰発現を招き、ヒトの遺伝病の原因となることがはじめて明らかとなった。HGの発症には多様な染色体微細構造異常が関与し、本症患者の重症度は当該患者において獲得されたプロモーターの機能と構造を反映すると推測される。

文　献

1) Shozu M, Sebastian S, Takayama K, Hsu WT, Schultz RA, Neely K, Bryant M, Bulun SE. Estrogen excess associated with novel gain-of-function mutations affecting the aromatase gene. N Engl J Med. 2003; 348: 1855-65

2) Demura M, Martin RM, Shozu M, Sebastian S, Takayama K, Hsu WT, Schultz RA, Neely K, Bryant M, Mendonca BB, Hanaki K, Kanzaki S, Rhoads DB, Misra M, Bulun SE. Regional rearrangements in chromosome 15q21 cause formation of cryptic promoters for the CYP19 (aromatase) gene. Hum Mol Genet. 2007; 16: 2529-41

J Clin Endocrin Metab. First published ahead of print April 6, 2011 as doi:10.1210/jc.2011-0145

Aromatase Excess Syndrome: Identification of Cryptic Duplications and Deletions Leading to Gain of Function of *CYP19A1* and Assessment of Phenotypic Determinants

Maki Fukami, Makio Shozu, Shun Soneda, Fumiko Kato, Akemi Inagaki, Hiroshi Takagi, Keiichi Hanaki, Susumu Kanzaki, Kenji Ohyama, Tomoaki Sano, Toshinori Nishigaki, Susumu Yokoya, Gerhard Binder, Reiko Horikawa, and Tsutomu Ogata

Department of Molecular Endocrinology (M.F., S.S., F.K., T.O.), National Research Institute for Child Health and Development, Tokyo 157-8535, Japan; Department of Reproductive Medicine (M.S.), Graduate School of Medicine, Chiba University, Chiba 206-8670, Japan; Department of Diabetes and Endocrinology (A.I., H.T.), Nagoya Second Red Cross Hospital Nagoya 466-8650, Japan; Department of Women's and Children's Family Nursing (K.H.) and Division of Pediatrics and Perinatology (S.K.), Tottori University, Yonago 683-8503, Japan; Department of Pediatrics (K.O., T.S.), Interdisciplinary Graduate School of Medicine and Engineering, University of Yamanashi, Chuo 408-3898, Japan; Department of Pediatrics (T.N.), Osaka Police Hospital, Osaka 543-0035, Japan; Department of Medical Subspecialties (S.Y., R.H.), National Medical Center for Children and Mothers, Tokyo 157-8535, Japan; and Pediatric Endocrinology Section (G.B.), University Children's Hospital, Tuebingen 72076, Germany

Context: Aromatase excess syndrome (AEXS) is a rare autosomal dominant disorder characterized by gynecomastia. Although cryptic inversions leading to abnormal fusions between *CYP19A1* encoding aromatase and its neighboring genes have been identified in a few patients, the molecular basis remains largely unknown.

Objective: The objective of the study was to examine the genetic causes and phenotypic determinants in AEXS.

Patients: Eighteen affected males from six families participated in the study.

Results: We identified three types of heterozygous genomic rearrangements, *i.e.* a 79,156-bp tandem duplication involving seven of 11 noncoding *CYP19A1* exons 1, a 211,631-bp deletion involving exons 2–43 of *DMXL2* and exons 5–10 of *GLDN*, and a 165,901-bp deletion involving exons 2–43 of *DMXL2*. The duplicated exon 1 functioned as transcription start sites, and the two types of deletions produced the same chimeric mRNA consisting of *DMXL2* exon 1 and *CYP19A1* coding exons. The *DMXL2* exon 1 harbored a translation start codon, and the *DMXL2/CYP19A1* chimeric mRNA was identified in only 2–5% of *CYP19A1*-positive transcripts. This was in contrast to the inversion-mediated chimeric mRNA that had no coding sequence on the fused exon 1 and accounted for greater than 80% of *CYP19A1*-positive transcripts. *CYP19A1* was expressed in a limited number of tissues, whereas its neighboring genes involved in the chimeric mRNA formation were expressed widely.

Conclusions: This study provides novel mechanisms leading to gain of function of *CYP19A1*. Furthermore, it appears that clinical severity of AEXS is primarily determined by the tissue expression pattern of relevant genes and by the structural property of promoter-associated exons of chimeric mRNA. ***(J Clin Endocrinol Metab* 96: 0000–0000, 2011)**

ISSN Print 0021-972X ISSN Online 1945-7197
Printed in U.S.A.

doi: 10.1210/jc.2011-0145 Received January 18, 2011. Accepted March 22, 2011.

Abbreviations: AEXS, Aromatase excess syndrome; CGH, comparative genomic hybridization; E_2, estradiol; FISH, fluorescence *in situ* hybridization; hCG, human chorionic gonadotropin; LCL, lymphoblastoid cell line; NMD, nonsense-mediated mRNA decay; RACE, rapid amplification of cDNA ends; SF, skin fibroblast; T, testosterone.

Aromatase is a cytochrome P450 enzyme that plays a crucial role in the estrogen biosynthesis (1). It catalyzes the conversion of Δ4-androstendione into estrone and that of testosterone (T) into estradiol (E_2) in the placenta and ovary as well as in other tissues such as the fat, skin, bone, and brain (1). It is encoded by *CYP19A1* consisting of at least 11 noncoding exons 1 and nine coding exons 2–10 (Supplemental Fig. 1, published on The Endocrine Society's Journals Online web site at http://jcem.endojournals.org) (2, 3). Each exon 1 is accompanied by a tissue-specific promoter and is spliced alternatively onto a common splice acceptor site at exon 2, although some transcripts are known to contain two of the exons 1, probably due to a splice error (2, 4). Of the 11 exons 1, exon I.4 appears to play a critical role in the regulation of estrogen biosynthesis in males because this exon contains a major promoter for extragonadal tissues including the skin and fat (2).

Excessive *CYP19A1* expression causes a rare autosomal dominant disorder known as aromatase excess syndrome (AEXS) (5–8). AEXS is characterized by pre- or peripubertal onset gynecomastia, advanced bone age from childhood to the pubertal period, and short adult height in affected males (5–8). Affected females may show several clinical features such as macromastia, precocious puberty, irregular menses, and short adult height (6–8). In this regard, previous studies have identified four heterozygous cryptic inversions around *CYP19A1* in patients with AEXS (5, 8). Each inversion results in the formation of a chimeric gene consisting of a noncoding exon(s) of a neighboring gene (*CGNL1*, *MAPK6*, *TMOD3*, or *TLN2*) and coding exons of *CYP19A1*. Because this condition is predicted to cause aberrant *CYP19A1* expression in tissues in which each neighboring gene is expressed, such inversions have been regarded to be responsible for AEXS (5, 8).

However, such inversions have been revealed only in a few patients with AEXS, and, despite extensive studies, no other underlying genetic mechanisms have been identified to date (6, 8–10). Here we report novel genomic rearrangements in AEXS and discuss primary phenotypic determining factors in AEXS.

Patients and Methods

Patients

This study was approved by the Institutional Review Board Committee at the National Center for Child Health and Development and was performed after obtaining informed consent. We examined 18 male patients aged 8–69 yr (cases 1–18) from six unrelated families A-F (Fig. 1A). The probands were ascertained by bilateral gynecomastia (Fig. 1B) and the remaining 12 males by familial studies. Ten other males allegedly had gynecomastia. There were four obligatory carrier females.

Phenotypic assessment showed pre- or peripubertal onset gynecomastia in all cases, small testes and fairly preserved masculinization in most cases, obvious or relative tall stature in childhood and grossly normal or relative short stature in adulthood, and age-appropriate or mildly advanced bone ages (Table 1) (for detailed actual data, see Supplemental Table 1). Such clinical features, especially gynecomastia, tended to be milder in cases 1–4 from families A and B than in the remaining cases from families C-F. Fertility or spermatogenesis was preserved in all adult cases (≥20 yr). In addition, the obligatory carrier females from families B and D had apparently normal phenotype, and such females from families E and F exhibited early menarche (9.0 yr) and short adult stature (−2.8 SD), respectively.

Blood endocrine studies revealed that LH values were grossly normal at the baseline and variably responded to GnRH stimulation, whereas FSH values were low at the baseline and responded poorly to GnRH stimulation, even after preceding GnRH priming (Table 1) (for detailed actual data, see Supplemental Table 1) (see also Fig. 1C for the cases aged ≥15 yr). Δ^4-Androstendione, T, and dihydrotestosterone values were low or normal. A human chorionic gonadotropin (hCG) test indicated relatively low but normal T responses in five young cases. In most cases, estrone values were elevated, E_2 values were normal or elevated, and E_2/T ratios were elevated. These endocrine data were grossly similar among cases 1–18.

Aromatase inhibitor (anastrozole, 1 mg/d) was effective in all the four cases treated (Supplemental Table 1) (see also Fig. 1C for cases aged ≥15 yr). Gynecomastia was mitigated within 6 months of treatment, and endocrine data were ameliorated within 1 month of treatment.

Primers

Primers used in this study are shown in Supplemental Table 2.

CYP19A1 mRNA levels and aromatase activities

We analyzed relative mRNA levels of *CYP19A1* and catalytic activities of aromatase in skin fibroblasts (SF) and lymphoblastoid cell lines (LCL). mRNA were extracted by a standard method and were subjected to RT-PCR using a high capacity RNA-to-cDNA kit (Life Technologies, Carlsbad, CA). A relative amount of *CYP19A1* mRNA against *B2M* was determined by the real-time PCR method using the Taqman gene expression assay on ABI PRISM 7500fast (Life Technologies) (assay no. Hs00903411_m1 for *CYP19A1* and Hs99999907_m1 for *B2M*). PCR was performed in triplicate. Aromatase activity was determined by a tritium incorporation assay (11). In brief, the samples were incubated with androstenedione-2-^{3}H for 2 h, and ^3H_2O in the supernatant of the culture media was measured with a scintillation counter LSC-5100 (Aloka, Tokyo, Japan).

Sequence analysis of *CYP19A1*

Leukocyte or SF genomic DNA samples from the six probands and additional four male patients (Fig. 1A) were PCR amplified for the coding exons 2–10 and their flanking splice sites of *CYP19A1*. Subsequently the PCR products were subjected to direct sequencing from both directions on CEQ 8000 autosequencer (Beckman Coulter, Fullerton, CA).

Genome structure analysis

Oligonucleotide array-based comparative genomic hybridization (CGH) analyses were carried out using a custom-built

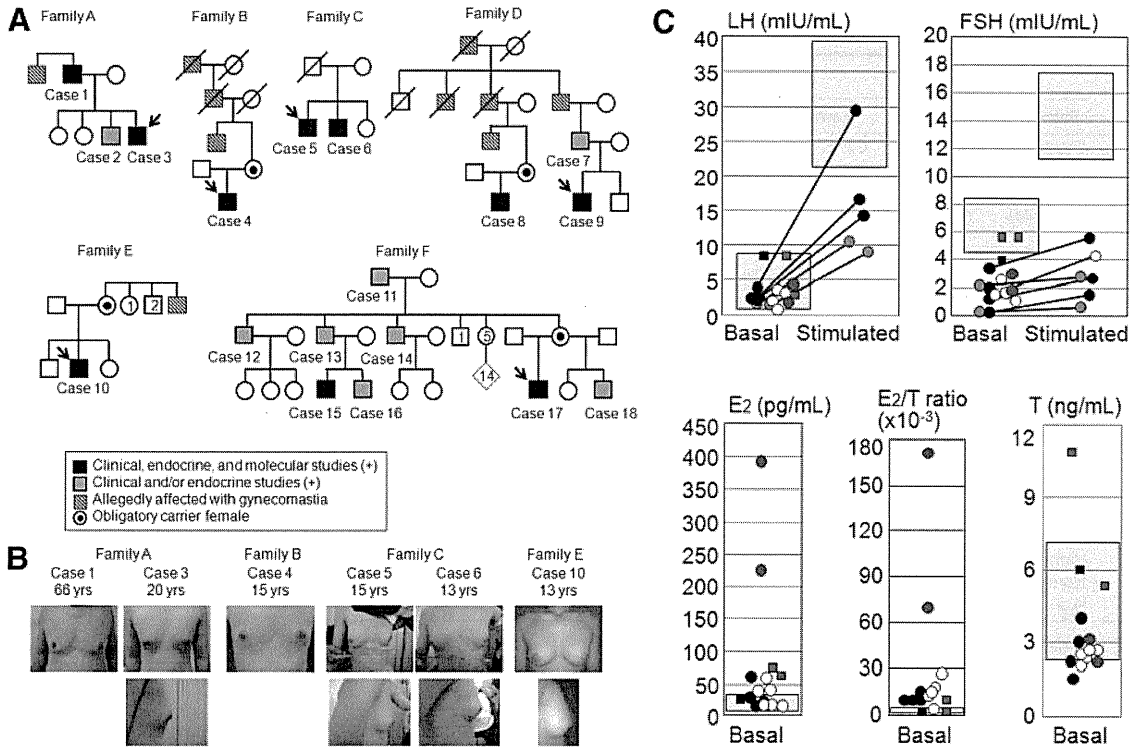

FIG. 1. Summary of clinical data. A, Pedigrees of six families with patients exhibiting AEXS-compatible phenotype. Families A–E are of Japanese origin, and family F is of German origin. Cases from families A–D were hitherto unreported, whereas those from families E and F have previously been described as having AEXS phenotypes (6, 8). B, Gynecomastia of six cases. C, Endocrine data in cases 15 yr of age or older. The *black*, *white*, and *red colors* represent the data in cases of the duplication, the deletion, and the inversion types, respectively; the *blue color* indicates the data of GnRH test after GnRH priming in two cases of the duplication type. The data at the time of diagnosis are denoted by *circles*, and those on aromatase inhibitor (anastrozole) treatment (1 mg/d in the duplication and the deletion types and 2–4 mg/d in the inversion types) are depicted by *squares*. The *light purple areas* represent the normal reference ranges.

oligo-microarray containing 90,000 probes for the 15q11.2-q26.3 region and approximately 10,000 reference probes for other chromosomal region (2 × 105K format, design identification 026533) (Agilent Technologies, Palo Alto, CA). The procedure was as described in the manufacturer's instructions. Fluorescence *in situ* hybridization (FISH) analysis was performed for lymphocyte or SF metaphase spreads, using long PCR products (FISH probes 1 and 2) for rearranged regions and CEP 15 probe for *D15Z4* used as an internal control (Abbott, Abbott Park, IL). The FISH probes 1 and 2 were labeled with digoxigenin and detected by rhodamine antidigoxigenin, and the CEP 15 probe was detected according to the manufacturer's protocol.

Characterization of the duplications and deletions

The duplication junctions were determined by direct sequencing for standard PCR products obtained with a variety of combinations of primers hybridizing to different positions within the *CYP19A1* exons 1 region. The deletion junctions were identified by direct sequencing of the long PCR products obtained with primer pairs flanking the deletions. The sizes of duplications and the deletions were determined by comparing obtained sequences with NT_010194 sequences at the National Center for Biotechnology Information Database (http://www.ncbi.nlm.nih.gov/; Bethesda, MD). The presence or absence of repeat sequences around the breakpoints was examined with Repeatmasker (http://www.repeatmasker.org).

For mRNA analysis, we preformed 5′-rapid amplification of cDNA ends (RACE) using a SMARTER RACE cDNA amplification kit (Takara Bio, Ohtsu, Japan). For both duplications and deletions, first PCR was carried out using the forward primer mix provided in the kit (Universal primer A mix) and an antisense reverse primer specific to *CYP19A1* exon 3 (RACE Rev). Second PCR was carried out for diluted products of the first PCR, using the nested forward primer of the kit (Nested universal primer A) and a reverse primer for *CYP19A1* exon 2 (Nested Rev). For duplications, furthermore, second PCR was also performed using various combinations of primers hybridizing to each *CYP19A1* exon 1. Subsequently PCR products were subcloned into TOPO cloning vector (Life Technologies) and subjected to direct sequencing. Then, the obtained sequences were examined with BLAST Search (National Center for Biotechnology Information). The presence or absence of promoter-compatible sequences was analyzed with the University of California, Santa Cruz, genome browser (http://genome.ucsc.edu/).

Relative mRNA levels of *CYP19A1* and its neighboring genes

We investigated relative mRNA levels of *CYP19A1* and *DMXL2* as well as those of *CGNL1*, *MAPK6*, *TMOD3*, and *TLN2* involved in the previously reported cryptic inversions (5, 8) in various human tissues. In this experiment, cDNA of SF and LCL were obtained from control males, and the remaining human cDNA samples were purchased from Life Technologies or Takara Bio. Relative quantification of mRNA against *TBP* was carried out using Taqman gene expression assay kit

TABLE 1. Summary of clinical studies in male patients with aromatase excess syndrome[a]

	Present study						Previous studies			
	Family A	Family B	Family C	Family D	Family E	Family F	Family 1	Family 2	Sporadic	
Cases	Cases 1–3	Case 4	Cases 5–6	Cases 7–9	Case 10	Cases 11–18	Two cases[b]	Proband[c]	Patient 1	Patient 2
Mutation type	Duplication	Duplication	Deletion	Deletion	Deletion	Deletion	Inversion	Inversion	Inversion	Inversion
Phenotypic findings										
Gynecomastia	Yes (mild)	Yes (mild)	Yes (moderate)	Yes (moderate)	Yes (moderate)	Yes (moderate)	Yes (severe)	Yes (severe)	Yes (severe)	Yes (severe)
Pubertal defect	Yes (mild)	Yes (mild)	Yes (mild)	No	No	Yes (mild)	N.D.	Yes (mild)	No	N.D.
Short adult height	No	No	N.D.	No	N.D.	No	Yes	N.D.	Yes	N.D.
Spermatogenesis	Preserved	N.D.	N.D.	Preserved	N.D.	Preserved	Preserved	N.D.	N.D.	N.D.
Endocrine findings										
LH (basal)	Normal	Normal	Normal	Normal/low	Normal	Normal/low	Normal	Normal/low	Normal	N.E.
LH (GnRH stimulated)[d]	Low	Normal	High	Normal	Normal	Normal	N.E.	Low	N.E.	N.E.
FSH (basal)	Low	Low	Low	Low	Low	Normal/low	Normal/low	Low	Low	N.E.
FSH (GnRH stimulated)[d]	Low	Low	Low	Low	Low	Low	N.E.	Low	N.E.	N.E.
T (basal)	Normal/low	Normal	Normal/low	Normal/low	Normal	Normal/low	Normal	Normal/low	Low	N.E.
T (hCG stimulated)[e]	N.E.	N.E.	Normal	Normal	Normal	Normal	N.E.	Normal	N.E.	N.E.
E_1 (basal)	High	High	N.E.	High	High	High	High	High	High	N.E.
E_2 (basal)	Normal	High	High	Normal	High	Normal/high	High	High	High	N.E.
E_2 to T ratio	High	High	High	High	High	High	High	High	High	N.E.

E_1, Estrone; N.D., not determined; N.E., not examined.

[a] Detailed actual data are shown in Supplemental Table 1.

[b] A father-son pair.

[c] The sister has macromastia, large uterus, and irregular menses; the parental phenotype has not been described.

[d] GnRH 100 $\mu g/m^2$ (maximum 100 μg) bolus iv; blood sampling at 0, 30, 60, 90, and 120 min.

[e] hCG 3000 IU/m^2 (maximum 5000 IU) im for 3 consecutive days; blood sampling on d 1 and 4.

(assay no. Hs00903411_m1 for *CYP19A1*; Hs00324048_m1 for *DMXL2*; Hs00262671_m1 for *CGNL1*; Hs00833126_g1 for *MAPK6*; Hs00205710_m1 for *TMOD3*; Hs00322257_m1 for *TLN2*; and Hs99999910_m1 for *TBP*). The experiments were carried out three times.

Results

CYP19A1 mRNA levels and aromatase activities

Although relative mRNA levels of *CYP19A1* and catalytic activities of aromatase were grossly similar between LCL of case 3 (family A), case 4 (family B), and case 5 (family C) and those of control subjects, they were significantly higher in SF of case 3 (family A), case 4 (family B), case 9 (family D), and case 10 (family E) than in those of control subjects (Fig. 2).

Sequence analysis of *CYP19A1*

Direct sequencing showed no mutation in *CYP19A1* coding exons 2–10 of the 10 cases examined.

Genome structure analysis

CGH analysis revealed heterozygous cryptic duplications involving most of the *CYP19A1* exons 1 region in cases from families A and B, heterozygous cryptic deletions involving most of *DMXL2* and part of *GLDN* in cases from family C, and heterozygous cryptic deletions involving most of *DMXL2* in cases from families D–F (Fig. 3A). FISH analysis supported the duplications and confirmed the deletions.

Characterization of the cryptic duplications

Aberrant PCR products were obtained with the P2 primer (which amplifies a segment between exon I.1 and exon IIa with the P1 primer) and the P3 primer (which amplifies a segment between exon I.2 and exon I.6 with the P4 primer), and sequencing of the PCR products showed the same tandem duplication involving seven of the 11 exons 1 of *CYP19A1* in cases from families A and B (Fig. 3B). The duplicated region was 79,156-bp long, and the

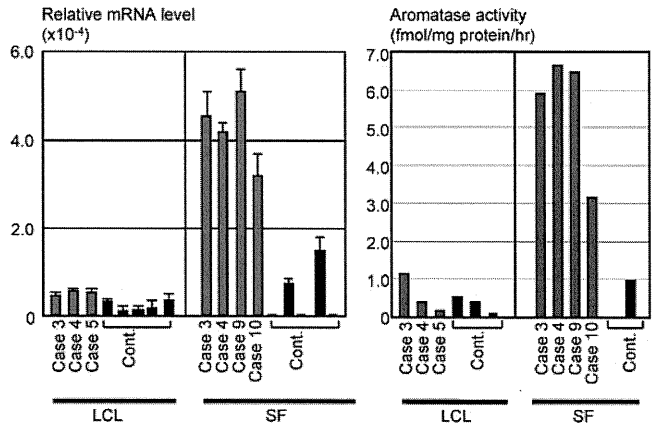

FIG. 2. Relative *CYP19A1* mRNA levels against *B2M* and catalytic activities of aromatase.

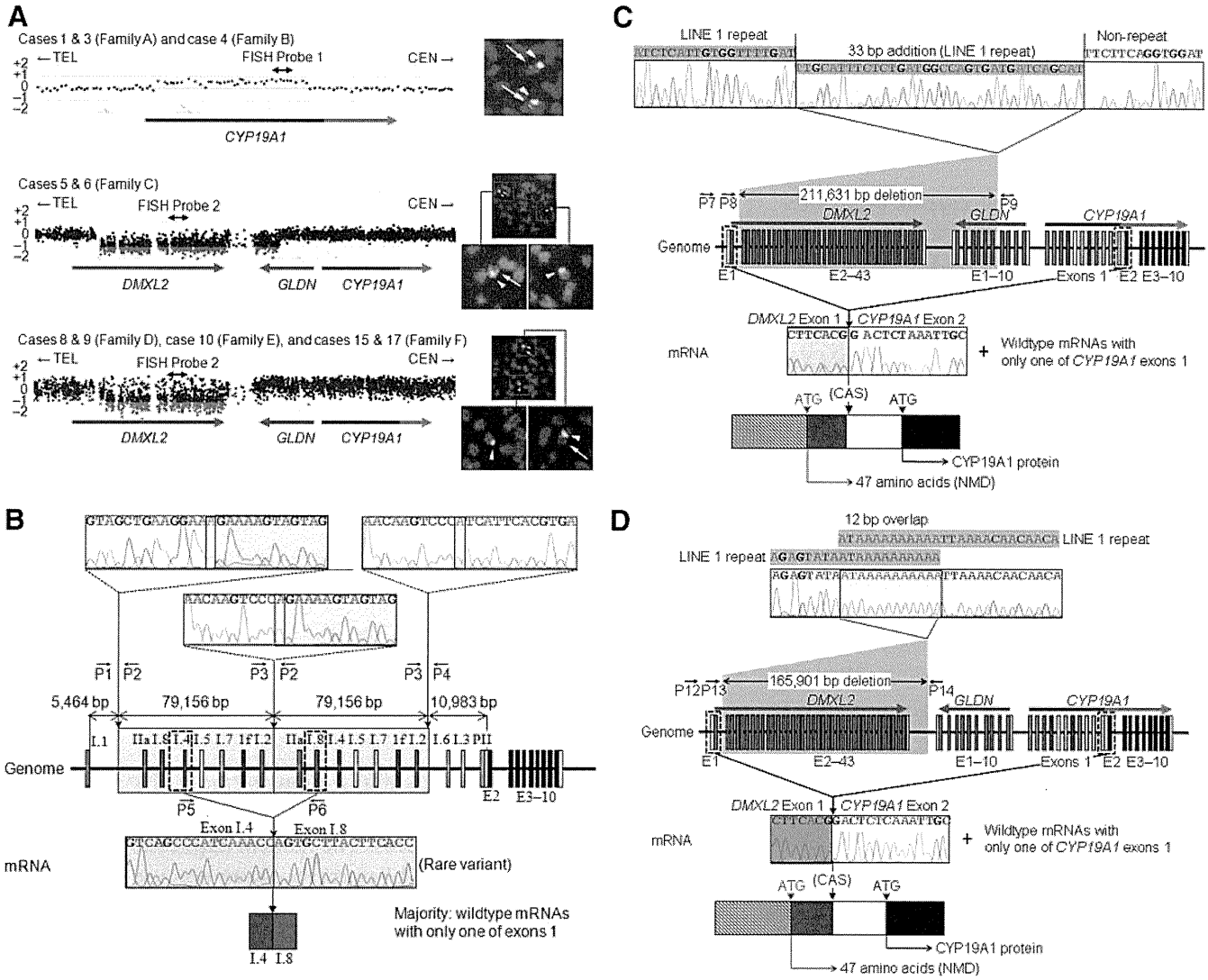

FIG. 3. Summary of molecular studies. For *CYP19A1*, the *dark* and *light blue lines* represent the genomic regions for noncoding exons 1 and coding exons 2–10, respectively. A, Oligoarray CGH and FISH analyses. In CGH analysis, the *black*, *red*, and *green dots* denote signals indicative of the normal, the increased (>+0.5), and the decreased (<−1.0) copy numbers, respectively. In FISH analysis, *two red signals* with an apparently different density are identified in cases from families A and B by FISH probe 1, whereas only a *single red signal* is found in cases from families C–F by FISH probe 2. The *green signals* are derived from the internal control probe. B, Schematic representation of the tandem duplication shared in common by cases 1 and 3 from family A and case 4 from family B. Genome, The junction sequence of the tandem duplication (*yellow boxes*) is shown, together with the original normal sequences at the 5′- and the 3′-ends of the duplicated region. The sequences highlighted with *light green* and *light orange* are identical, and 1 bp (A) is shared at the junction point (highlighted with *light yellow*). mRNA, The sequence of a rare clone is shown. The 3′-end of exon I.4 is connected with the 5′-end of exon I.8. C, Schematic representation of the deletion in sibling cases 5 and 6 from family C. Genome, The junction sequence of the deletion (*a gray area*) is shown. The fusion has occurred between a LINE 1 repeat sequence (*highlighted with blue*) at intron 1 of *DMXL2* and a nonrepeat sequence at intron 4 of *GLDN* and is accompanied by an addition of a 33-bp segment with a LINE 1 repeat sequence. mRNA, The sequence of a rare chimeric gene transcript is shown. *DMXL2* exon 1 consisting of a noncoding region (a *red striped box*) and a coding region (a *red box*) is spliced onto the common acceptor site (CAS) of *CYP19A1* exon 2 comprising an untranslated region (a *white box*) and a coding region (a *black box*). Thus, this transcript has two translation initiation codons (ATG), although the mRNA destined to produce a 47-amino acid protein from the ATG on *DMXL2* exon 1 is predicted to undergo NMD. D, Schematic representation of the deletion shared in common by cases 8 and 9 from family D, case 10 from family E, and cases 15 and 17 from family F. Genome, The junction sequence of the deletion (a *gray area*) is shown. The fusion has occurred between a LINE 1 repeat sequence (*highlighted with blue*) at intron 1 of *DMXL2* and that at a downstream region of *DMXL2*, with an overlap of a 12-bp segment. mRNA, The sequence of a chimeric gene transcript is delineated. The mRNA structure is the same as that described in the legend for Fig. 3C.

fusion occurred between nonrepeat elements with an overlap of one nucleotide.

All the 5′-RACE products (>500 clones) obtained from LCL and SF of case 3 (family A) and case 4 (family B) were found to be associated with a single exon 1, as observed in control materials. However, PCR amplifications for the 5′-RACE products with a variety of combinations of primers hybridizing to each exon 1 and subsequent sequencing of the PCR products revealed the presence of a chimeric clone consisting of exon I.4 at the 5′ side and exon I.8 at

the 3′ side in both LCL and SF (Fig. 3B). Although such a chimeric clone would have been produced by a splice error, this indicated that duplicated exon 1.4 at the distal nonphysiological position functioned as a transcription start site.

Characterization of the cryptic deletions

In cases from family C, long PCR products were obtained with the P7 primer and the P9 primer, and the deletion junction was determined by direct sequencing with the P8 primer (Fig. 3C). The deleted region was 211,631-bp long and involved exons 2–43 of *DMXL2* and exons 5–10 of *GLDN*. The two breakpoints resided within a LINE 1 repeat sequence and a nonrepeat sequence respectively, and a 33-bp segment with a LINE 1 repeat sequence was inserted to the fusion point. In cases from families D–F, long PCR products were obtained by sequential amplifications with the P12 primer and the P14 primer and with the P13 primer and the P14 primer, and an identical deletion was identified by direct sequencing with the P13 primer (Fig. 3D). The deletion was 165,901-bp long and involved exons 2–43 of *DMXL2*. The fusion occurred between two LINE 1 repeat sequences with an overlap of a 12-bp segment.

Sequence analysis of the 5′-RACE products obtained from LCL of cases 5 and 6 (family C) and from SF of case 9 (family D) and case 10 (family E) revealed the presence of a few clones with *DMXL2* exon 1 (2–5%), together with multiple clones with a single wild-type *CYP19A1* exon 1 (Fig. 3, C and D). Such a chimeric mRNA clone was absent from control materials. Furthermore, *DMXL2* exon 1 was found to be accompanied by a promoter-compatible sequence (Supplemental Fig. 2). This indicated a cryptic usage of *DMLX2* exon 1 as an alternative *CYP19A1* transcription start site in cases with deletions. Notably, because of the presence of the translation start codon on *DMXL2* exon 1, mRNAs of the *DMLX2/CYP19A1* chimeric genes are predicted to produce two proteins, *i.e.* CYP19A1 protein and an apparently nonfunctional 47-amino acid protein with a termination codon on *CYP19A1* exon 2, when the translation started from the initiation codons on *CYP19A1* exon 2 and on *DMLX2* exon 1, respectively. Furthermore, mRNA destined to yield the 47-amino acid protein is predicted to undergo nonsense-mediated mRNA decay (NMD) because it satisfies the condition for the occurrence of NMD (12).

Relative mRNA levels of *CYP19A1* and its neighboring genes

CYP19A1 showed a markedly high expression in the placenta and a relatively weak expression in a limited number of tissues including hypothalamus and ovary. By contrast, *DMXL2* was expressed in a range of tissues with some degree of variation as well as *CGNL1*, *MAPK6*, *TMOD3*, and *TLN2* (Fig. 4).

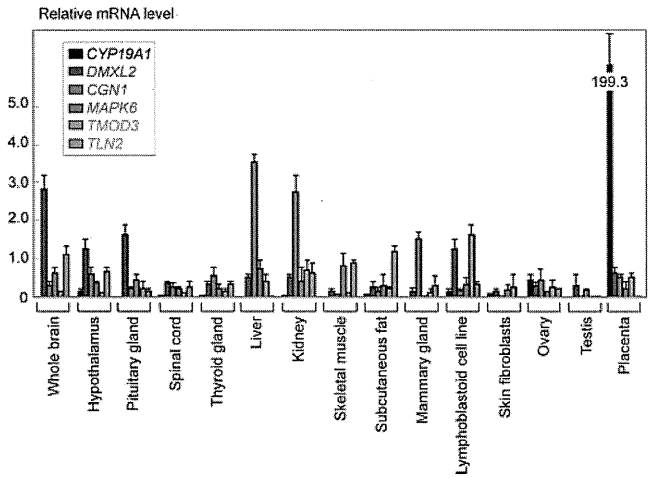

FIG. 4. Expression patterns of *CYP19A1* and the five neighboring genes involved in the chimeric gene formation. Relative mRNA levels against *TBP* are shown.

Discussion

We identified cryptic duplications of the *CYP19A1* promoter region and deletions of the *CYP19A1* upstream region in cases with AEXS. The tandem duplications would have caused *CYP19A1* overexpression because of an increased number of the wild-type transcription start sites. Indeed, because a rare mRNA variant with exon I.4 and exon I.8 was identified, this implies that duplicated exons 1 at the distal nonphysiological position can also function as transcription start sites. Similarly, the deletions would have caused *CYP19A1* overexpression because of a cryptic usage of *DMXL2* exon 1 with a putative promoter function as an extra transcription start site for *CYP19A1*. Indeed, because a few clones with *DMXL2* exon 1 and *CYP19A1* exon 2 were identified, this confirms the formation of a *DMXL2/CYP19A1* chimeric gene. Thus, our results suggest for the first time that duplications of a physiological promoter and deletions of an upstream region can cause overexpression of a corresponding gene and resultant human genetic disease.

Such cryptic genomic rearrangements can be generated by several mechanisms. The tandem duplication in families A and B would be formed by a replication-based mechanism of fork stalling and template switching that occurs in the absence of repeat sequences and is associated with microhomology (13). The deletion in family C is explained by nonhomologous end joining that takes place between nonhomologous sequences and is frequently accompanied by an insertion of a short segment at the fusion point (13).

The deletion in families D–F is compatible with a repeat sequence mediated nonallelic intrachromosomal or interchromosomal recombination (13). Thus, in conjunction with the previously identified four cryptic inversions that are also explainable by fork stalling and template switching or nonallelic recombination (8), genomic sequence around *CYP19A1* appears to harbor particular motifs that are vulnerable to replication and recombination errors.

To date, three types of cryptic genomic rearrangements have been identified in patients with AEXS, *i.e.* duplication type, deletion type (two subtypes), and inversion type (four subtypes) (Fig. 5). Here, although the deletion and the inversion types are associated with heterozygous impairment of neighboring genes (deletion or disconnection between noncoding exon(s) and coding exons), the phenotypes of patients are well explained by excessive *CYP19A1* activity alone. Thus, haploinsufficiency of these neighboring genes would not have a major clinical effect.

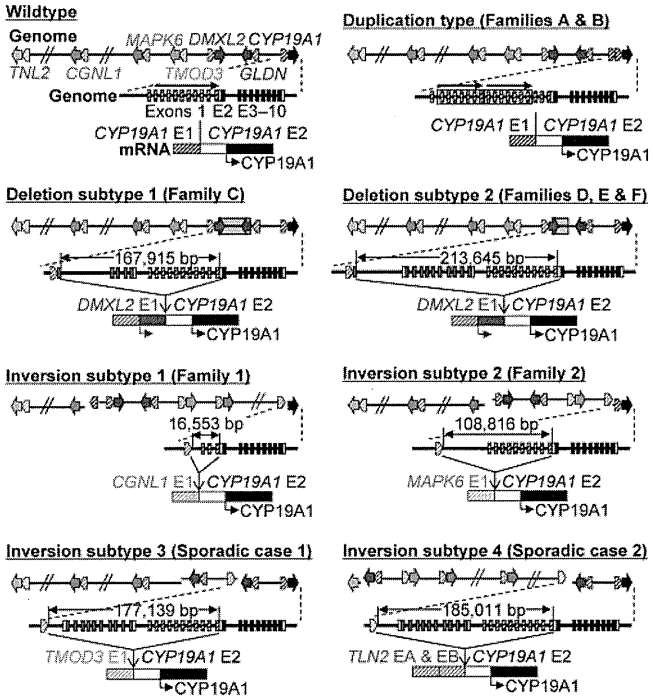

FIG. 5. Schematic representation of the rearranged genome and mRNA structures. The *white* and *black boxes* of *CYP19A1* exon 2 show untranslated region and coding region, respectively (for details, see Supplemental Fig. 1). For the duplication type and the deletion subtypes, see Fig. 3, C and D, for details. For genome, the *striped* and *painted arrows* indicate noncoding and coding exons, respectively (5′→3′). The inverted genomic regions are delineated in *blue lines*. For mRNA, *colored striped boxes* represent noncoding regions of each gene. For *TLN2*, exons A and B correspond to the previously reported exons 1 and 2 (8); because current exon 1 in the public database indicates the first coding exon, we have coined the terms exons A and B for the noncoding exons. The deletion and inversion types are associated with heterozygous impairment of neighboring genes [deletion or disconnection between noncoding exon(s) and the following coding exons]. The inversion subtype 1 is accompanied by inversion of eight of the 11 *CYP19A1* exons 1, and the inversion subtype 2 is associated with inversion of the placenta-specific *CYP19A1* exon I.1.

For the deletion and inversion types, two factors should be considered. One factor is expression patterns of each chimeric gene. In this regard, the five genes involved in the formation of chimeric genes are widely expressed, with some degree of variation (Fig. 4). Furthermore, *in silico* analysis revealed promoter-compatible sequences around exon 1 of *DMXL2*, *CGN1*, *MAPK6*, and *TMOD3* in multiple cell types, although such sequences remain to be identified for noncoding exons of *TLN2* (Supplemental Fig. 2). These findings imply that the chimeric genes show wide expression patterns because expression patterns of chimeric genes would follow those of the original genes.

The other factor is expression dosage of each chimeric gene. In this context, the *DMXL2/CYP19A1* chimeric mRNA was identified only in 2–5% of transcripts from SF, whereas the *CGNL1/CYP19A1* chimeric mRNA and the *TMOD3/CYP19A1* chimeric mRNA accounted for 89–100% and 80% of transcripts from SF, respectively (no data for the *MAPK6/CYP19A1* and the *TLN2/CYP19A1* chimeric genes) (5). This difference is obviously inexplicable by the relative expression level in SF that is grossly similar between *DMXL2* and *TMOD3* and is quite low for *CGNL1* (Fig. 4). In this regard, it is notable that a translation start codon and a following coding region are present on exon 1 of *DMXL2* (Fig. 5). It is likely that *DMXL2/CYP19A1* chimeric mRNA transcribed by the *DMXL2* promoter preferentially recognized the natural start codon on *DMXL2* exon 1 and underwent NMD and that rather exceptional chimeric mRNAs, which recognized the start codon on *CYP19A1* exon 2, were identified by 5′-RACE. By contrast, such a phenomenon would not be postulated for the inversion-mediated chimeric mRNA because of the absence of a translation start codon on the fused exon 1 of *CGNL1* and *TMOD3* (as well as exon 1 of *MAPK6* and exons A and B of *TLN2*) (Fig. 5). For the *CGNL1/CYP19A1* chimeric gene, furthermore, the physical distance between *CGNL1* exon 1 and *CYP19A1* exon 2 is short, and whereas a splice competition may be possible between exon 1 of neighboring genes and original *CYP19A1* exons 1, eight of 11 *CYP19A1* exons 1 including exon I.4 functioning as the major promoter in SF have been disconnected from *CYP19A1*-coding exons by inversion. These structural characters would have also contributed to the efficient splicing between *CGNL1* exon 1 and *CYP19A1* exon 2 (14). In this context, although the *CGNL1/CYP19A1* chimeric gene is associated with functional loss of eight *CYP19A1* exons 1 and the resultant reduction of *CYP19A1* expression in *CYP19A1*-expressing tissues, overall aromatase activity would be increased

by the wide expression of the chimeric gene. These structural properties would primarily explain the difference in the expression dosage of chimeric mRNA between the deletion and the inversion types.

It is inferred, therefore, that the duplication type simply increases *CYP19A1* transcription in native *CYP19A1*-expressing tissues, whereas the deletion and the inversion types cause relatively mild and severe *CYP19A1* overexpression in a range of tissues, respectively. These notions would grossly explain why clinical features of affected males and carrier females and endocrine profiles of affected males are apparently milder in the duplication and the deletion types than in the inversion type and why clinical findings were ameliorated with 1 mg/d of anastrozole in the duplication and the deletion types and with 2–4 mg/d of anastrozole in the inversion type. In addition, the different expression pattern between *CYP19A1* and *DMXL2* may explain, in terms of autocrine and/or paracrine effects, why phenotypic features such as gynecomastia tended to be more severe in the deletion type than in the duplication type under similar endocrine profiles.

Furthermore, several findings are notable in this study. First, a similar degree of FSH-dominant hypogonadotropic hypogonadism is present in the three types, with no amelioration of FSH responses to GnRH stimulation after GnRH priming in two cases with the duplication. This suggests that a relatively mild excess of circulatory estrogens, as observed in the duplication and the deletion types, can exert a strong negative feedback effect on FSH secretion, primarily at the pituitary, as has been suggested previously (15–19). Second, although basal T values appear to be mildly and similarly compromised in the three types, age-matched comparison suggests that T responses to hCG stimulation are apparently normal in the duplication and the deletion types and somewhat low in the inversion type. These data, although they remain fragmentary, would primarily be compatible with fairly preserved LH secretion in the three types and markedly increased estrogen values in the inversion type because T production is under the control of LH (1), and excessive estrogens compromise testicular steroidogenic enzyme activity (20, 21). Lastly, although testis volume appears somewhat small, fertility (spermatogenesis) is normally preserved in the three types. This would be consistent with the FSH-dominant hypogonadotropic hypogonadism because FSH plays only a minor role in male fertility (spermatogenesis) (22). Indeed, males with mutations of *FSHR* encoding FSH receptor as well as mice lacking *FSHB* or *FSHR* can be fertile (23, 24).

The results of this study are contrastive to those of the previous studies. In the previous studies, inversions only have been identified, and each inversion is specific to each family or patient (8). By contrast, in this study, the identical duplication was found in two Japanese families A and B, and the same deletion (subtype 2 in Fig. 5) was shared by three Japanese and one Caucasian families D–F, despite apparent nonconsanguinity. This may be explained by assuming that patients with severe phenotype were preferentially examined in the previous studies, whereas those with the AEXS phenotype were analyzed in this study without ascertainment bias. Furthermore, because phenotypes are milder in the duplication and the deletion types than in the inversion type, this may have permitted the spread of the duplication and the deletion types, but not the inversion type, as the founder abnormalities. This notion predicts that the duplication and the deletion types would be identified by examining patients with mild AEXS phenotype.

In summary, the present study shows that AEXS can be caused by duplications of the physiological promoters and microdeletions of the upstream regions of *CYP19A1* and that phenotypic severity is primarily determined by the tissue expression pattern of *CYP19A1* and the chimeric genes and by structural properties of the fused exons. Most importantly, the present study provides novel models for the gain-of-function mutations leading to human genetic disease.

Acknowledgments

Address all correspondence and requests for reprints to: Dr. Tsutomu Ogata, Department of Molecular Endocrinology, National Research Institute for Child Health and Development, 2-10-1 Ohkura, Setagaya, Tokyo 157-8535, Japan. E-mail: tomogata@nch.go.jp.

Present address for T.O.: Department of Pediatrics, Hamamatsu University School of Medicine, Hamamatsu 431-3192, Japan.

This work was supported by Grants for Research on Intractable Diseases (H22-035 and H22-098) from the Ministry of Health, Labor, and Welfare; Grants-in-Aid for Scientific Research (B) (20390265) and (S) (22227002) from the Japan Society for the Promotion of Science; and Grant-in-Aid for Scientific Research on Innovative Areas (22132004) from the Ministry of Education, Culture, Sports, Science, and Technology.

Disclosure Summary: The authors have nothing to declare.

References

1. **Bhasin S** 2008 Testicular disorders. In: Kronenberg HM, Melmed M, Polonsky KS, Larsen PR, eds. Williams textbook of endocrinology. 11th ed. Philadelphia: Saunders; 645–699
2. **Bulun SE, Takayama K, Suzuki T, Sasano H, Yilmaz B, Sebastian S**

2004 Organization of the human aromatase p450 (CYP19) gene. Semin Reprod Med 22:5–9
3. **Demura M, Reierstad S, Innes JE, Bulun SE** 2008 Novel promoter I. 8 and promoter usage in the CYP19 (aromatase) gene. Reprod Sci 15:1044–1053
4. **Harada N, Utsumi T, Takagi Y** 1993 Tissue-specific expression of the human aromatase cytochrome P-450 gene by alternative use of multiple exons 1 and promoters, and switching of tissue-specific exons 1 in carcinogenesis. Proc Natl Acad Sci USA 90:11312–11316
5. **Shozu M, Sebastian S, Takayama K, Hsu WT, Schultz RA, Neely K, Bryant M, Bulun SE** 2003 Estrogen excess associated with novel gain-of-function mutations affecting the aromatase gene. N Engl J Med 348:1855–1865
6. **Binder G, Iliev DI, Dufke A, Wabitsch M, Schweizer R, Ranke MB, Schmidt M** 2005 Dominant transmission of prepubertal gynecomastia due to serum estrone excess: hormonal, biochemical, and genetic analysis in a large kindred. J Clin Endocrinol Metab 90: 484–492
7. **Martin RM, Lin CJ, Nishi MY, Billerbeck AE, Latronico AC, Russell DW, Mendonca BB** 2003 Familial hyperestrogenism in both sexes: clinical, hormonal, and molecular studies of two siblings. J Clin Endocrinol Metab 88:3027–3034
8. **Demura M, Martin RM, Shozu M, Sebastian S, Takayama K, Hsu WT, Schultz RA, Neely K, Bryant M, Mendonca BB, Hanaki K, Kanzaki S, Rhoads DB, Misra M, Bulun SE** 2007 Regional rearrangements in chromosome 15q21 cause formation of cryptic promoters for the CYP19 (aromatase) gene. Hum Mol Genet 16:2529–2541
9. **Tiulpakov A, Kalintchenko N, Semitcheva T, Polyakov A, Dedov I, Sverdlova P, Kolesnikova G, Peterkova V, Rubtsov P** 2005 A potential rearrangement between CYP19 and TRPM7 genes on chromosome 15q21.2 as a cause of aromatase excess syndrome. J Clin Endocrinol Metab 90:4184–4190
10. **Stratakis CA, Vottero A, Brodie A, Kirschner LS, DeAtkine D, Lu Q, Yue W, Mitsiades CS, Flor AW, Chrousos GP** 1998 The aromatase excess syndrome is associated with feminization of both sexes and autosomal dominant transmission of aberrant P450 aromatase gene transcription. J Clin Endocrinol Metab 83:1348–1357
11. **Bellino FL, Osawa Y** 1977 Localization of estrogen synthetase in the chorionic villus fraction after homogenization of human term placenta. J Clin Endocrinol Metab 44:699–707
12. **Kuzmiak HA, Maquat LE** 2006 Applying nonsense-mediated mRNA decay research to the clinic: progress and challenges. Trends Mol Med 12:306–316
13. **Gu W, Zhang F, Lupski JR** 2008 Mechanisms for human genomic rearrangements. Pathogenetics 1:4
14. **Castillo-Davis CI, Mekhedov SL, Hartl DL, Koonin EV, Kondrashov FA** 2002 Selection for short introns in highly expressed genes. Nat Genet 31:415–418
15. **Shaw ND, Histed SN, Srouji SS, Yang J, Lee H, Hall JE** 2010 Estrogen negative feedback on gonadotropin secretion: evidence for a direct pituitary effect in women. J Clin Endocrinol Metab 95:1955–1961
16. **Belgorosky A, Guercio G, Pepe C, Saraco N, Rivarola MA** 2009 Genetic and clinical spectrum of aromatase deficiency in infancy, childhood and adolescence. Horm Res 72:321–330
17. **Alexander DC, Miller WL** 1982 Regulation of ovine follicle-stimulating hormone β-chain mRNA by 17β-estradiol *in vivo* and *in vitro*. J Biol Chem 257:2282–2286
18. **Mercer JE, Clements JA, Funder JW, Clarke IJ** 1988 Luteinizing hormone-β mRNA levels are regulated primarily by gonadotropin-releasing hormone and not by negative estrogen feedback on the pituitary. Neuroendocrinology 47:563–566
19. **Raven G, de Jong FH, Kaufman JM, de Ronde W** 2006 In men, peripheral estradiol levels directly reflect the action of estrogens at the hypothalamo-pituitary level to inhibit gonadotropin secretion. J Clin Endocrinol Metab 91:3324–3328
20. **Moger WH** 1980 Direct effects of estrogens on the endocrine function of the mammalian testis. Can J Physiol Pharmacol 58:1011–1022
21. **Strauss L, Kallio J, Desai N, Pakarinen P, Miettinen T, Gylling H, Albrecht M, Mäkelä S, Mayerhofer A, Poutanen M** 2009 Increased exposure to estrogens disturbs maturation, steroidogenesis, and cholesterol homeostasis via estrogen receptor α in adult mouse Leydig cells. Endocrinology 150:2865–2872
22. **Kumar TR, Wang Y, Lu N, Matzuk MM** 1997 Follicle stimulating hormone is required for ovarian follicle maturation but not male fertility. Nat Genet 15:201–204
23. **Tapanainen JS, Aittomäki K, Min J, Vaskivuo T, Huhtaniemi IT** 1997 Men homozygous for an inactivating mutation of the follicle-stimulating hormone (FSH) receptor gene present variable suppression of spermatogenesis and fertility. Nat Genet 15:205–206
24. **Layman LC, McDonough PG** 2000 Mutations of follicle stimulating hormone-β and its receptor in human and mouse: genotype/phenotype. Mol Cell Endocrinol 161:9–17

Ⅳ. その他資料

表１　遺伝性女性化乳房症の診断の手引き（案）

遺伝性女性化乳房

遺伝性女性化乳房は、性腺外組織で過剰に産生されたエストロゲンにより男性に女性化乳房・低身長などの症状をもたらす常染色体優性の遺伝性疾患である。これまでに、アロマターゼ遺伝子に構造異常をもつ家系が知られている。アロマターゼ阻害剤投与により症状の発生を抑制できる可能性があることから、早期診断が望まれる。

診断の手引き

診断項目１）～４）の項目を満たすものを、臨床的に遺伝性女性化乳房と診断する。同意を得て、末梢血白血球の細胞遺伝学的検査により診断を確定する。１）～３）を満たすが、４）を満たさないものは疑い例とし、細胞遺伝学的検査により診断を確定する。血中ホルモン値は、診断の参考にとどめ、診断基準には含めない。

A. 診断項目

１）タナー分類２度以上の両側性乳房発育[注1)]

２）発症年齢が 20 歳以下[注2)]

３）２次性女性化乳房[注3)]と思春期一過性女性化乳房症[注4)]を除外できる

４）家系内発症がある[注5)]

B. 参考とする内分泌検査

- 血中エストラジオール(E2)：

  高値例が多いが、高値を示さない症例も存在する。E2 値から本症の可能性を除外することはできない。

- E2／テストステロン比：

  T から E2 への転換率を反映する。遺伝性女性化乳房症では、E2[pg/ml]/T[ng/ml](T)＞10 を示す例が多いが、その他の疾患（クラインフェルター症候群、肝疾患など）でも E2/T＞10 となることがある。

- 血中ゴナドトロピン：

  FSH 低値、LH 基準値のことが多い。

● アロマターゼ活性：

乳腺組織のアロマターゼ活性が、同年齢の健常者に比し高値を示す。乳腺以外の皮下脂肪や血中単核球のアロマターゼ活性も、高値を示す例が多い。

C. 細胞遺伝学的検査

末梢血白血球ゲノムDNAを用いてアロマターゼ遺伝子の変異を同定する[注6)]。乳腺もしくは皮膚より採取した組織から細胞を分離して、アロマターゼ活性を測定することもできる。末梢血単球で代用できることもある。

注記

注 1) 乳房腫大は進行性である。腫大の程度は遺伝子型と相関しており、遺伝子変異型によっては、乳房腫大が軽度にとどまる家系もある。両側の腫大を示すが、腫大の程度に左右差がある例もある。女性例では、巨大乳房として認識される。

注 2) 思春期、遅くとも 20 歳までに発症（乳房腫大を自覚または他覚）する。前思春期から、乳房腫大が始まる例がある。

注 3) 二次性女性化乳房（付表）の可能性を除外する。二次性女性化乳房では、それぞれ原疾患の所見や兆候があるのに対し、遺伝性女性化乳房ではエストロゲン高値に基づく乳房腫大・低身長症状以外の症状を示さない。

注 4) 思春期男児には、生理的な一過性両側性乳房腫大がしばしば見られる。発症時期が思春期である、症状（乳房の増大や疼痛）の進行がおおむね 1 年以内で止まりその後軽快に向かうなどの所見は、一過性乳房腫大を示唆する。

注 5) 家系内発生があれば、本症である可能性が高い。父親に女性化乳房がみられる症例が多い。家系発生が確認できない場合でも、本症を確実に否定することはできない。母方の遺伝で巨大乳房が自覚されていない、de novo に発生した弧発例などの可能性がある。細胞遺伝学的検索、もしくは乳腺組織のアロマターゼ活性測定により診断を確定する。

注 6) 5'-rapid amplification of cDNA ends, 5'RACE（プロモーター逆位）、15 番染色体 comparative genomic hybridization (CGH)オリゴプローブアレイ(重複、欠失)、fluorescence in situ hybridization, FSH 等により変異を検出し、シークエンス等により確定する。

表２　別表　女性化乳房の原因

症候性（２次性）	A. 染色体異常	A1. Klinefelter 症候群 A2. XX 男性、Swyer 症候群 A3. その他
	B. 酵素欠損症	B1. 3β-HSD 欠損症 B2. 21-hydroxylase 欠損症 B3. 17α-hydroxylase 欠損症 B3. その他
	C. アンドロゲン受容体関連異常症	C1. アンドロゲン不応症 C2. その他
	D. 神経筋疾患	D1. 球脊髄性筋萎縮症（Kennedy-Alter-Sung 症候群） D2. POEMS 症候群（Crow-Fukase 症候群） D3. 筋強直性ジストロフィー D4. ミトコンドリア脳筋症 D5. 筋ジストロフィー D6. その他
	E. 悪性腫瘍	E1. hCG 産生腫瘍（肺癌、胃癌、精巣腫瘍、尿路移行上皮癌など） E2. 絨毛癌（胃癌、縦隔腫瘍、膀胱癌、精巣腫瘍） E3. 胚細胞性腫瘍（精巣腫瘍、縦隔腫瘍） E4. エストロゲン産生腫瘍（胃癌、精巣腫瘍、副腎腫瘍） E5. 肝細胞癌 E6. Peutz-Jeghers 症候群 E7. 悪性リンパ腫 E8. 多発性内分泌腫瘍 E9. その他
	F. 内分泌疾患	F1. 甲状腺機能亢進症 F2. 低ゴナドトロピン性性腺機能低下症 F3. 高ゴナドトロピン血症 F4. GH 分泌不全症 F5. ACTH 単独欠損症 F6. 高プロラクチン血症 F7. その他
	G. 肝疾患	G1. 肝硬変 G2. その他
	H. 腎疾患	H1. 透析 H2. その他
	I. 薬剤性	I1. アルドステロン拮抗薬 I2. 降圧剤 I3. 抗精神薬 I4. 制酸剤 I5. ホルモン剤 I6. 抗 HIV 薬 I7. 高脂血症薬 I8. 漢方薬（牛車腎気丸） I9. 牛乳 I10. その他　(male to female などを含む)
特発性（原発性）	J. 特定の原因が見あたらないもの（２次性でない）	J1. 家族性・遺伝性がない J2. 家族性・遺伝性がある(推定も含む) [家系内に女性化乳房患者がいる場合など] J3. 家族歴・遺伝歴が不明 J4. その他